Biogeosciences Discuss., 9, 13685–13712, 2012
www.biogeosciences-discuss.net/9/13685/2012/
doi:10.5194/bgd-9-13685-2012

Biogeosciences Discussions

GCM characteristics explain the majority of uncertainty in projected 21st century terrestrial ecosystem carbon balance

A. Ahlström[1], J. Lindström[2], M. Rummukainen[3], B. Smith[1], and C. B. Uvo[4]

[1]Department of Physical Geography and Ecosystem Science, Lund University, Sölvegatan 12, 223 62 Lund, Sweden
[2]Mathematical Statistics, Centre for Mathematical Sciences, Lund University, Box 118, 22100, Lund, Sweden
[3]Centre for Environmental and Climate Research, Lund University, Sölvegatan 37, 223 62 Lund, Sweden
[4]Department of Water Resource Engineering, LTH, Lund University, Box118, 22100 Lund, Sweden

Received: 20 August 2012 – Accepted: 17 September 2012 – Published: 8 October 2012

Correspondence to: A. Ahlström (anders.ahlstrom@nateko.lu.se)

Published by Copernicus Publications on behalf of the European Geosciences Union.

Abstract

One of the largest sources of uncertainties in modelling of the future global climate is the response of the terrestrial carbon cycle. Studies have shown that it is likely that the extant land sink of carbon will weaken in a warming climate. Should this happen, a larger portion of the annual carbon dioxide emissions will remain in the atmosphere, and further increase the global warming, which in turn may further weaken the land sink. We investigate the potential sensitivity of global terrestrial ecosystem carbon balance to differences in future climate simulated by four general circulation models (GCMs) under three different CO_2 concentration scenarios. We find that the response in simulated carbon balance is more influenced by GCMs than CO_2 concentration scenarios. Singular Value Decomposition (SVD) analysis of sea surface temperatures (SSTs) reveals differences in the GCMs SST variability leading to decreased tropical ecosystem productivity in two out of four GCMs. We extract parameters describing GCM characteristics by parameterizing a statistical replacement model mimicking the simulated carbon balance results. By sampling two GCM-specific parameters and global temperatures we create 60 new "artificial" GCMs and investigate the extent to which the GCM characteristics may explain the uncertainty in global carbon balance under future radiative forcing. Our analysis suggests that differences among GCMs in the representation of SST variability and ENSO and its effect on precipitation and temperature patterns explains the majority of the uncertainty in the future evolution of global terrestrial ecosystem carbon.

1 Introduction

The discussion about climate change uncertainties has tended to focus on climate sensitivity, i.e. the global mean warming induced by increased atmospheric CO_2 concentration ($[CO_2]$), which differs among climate models (atmosphere-ocean general circulation models, AOGCMs, hereafter "GCM") depending on the assumed strength

BGD
9, 13685–13712, 2012

and sign of feedbacks that may dampen or amplify the direct radiative forcing of CO_2 through the greenhouse effect (Knutti and Hegerl, 2008). However, the terrestrial biosphere and surface layers of the oceans together sequester almost two-thirds of anthropogenic CO_2 emissions, and the fate of these sinks in future decades constitutes a major additional source of uncertainty, not accounted for by the current generation of GCMs (Canadell et al., 2007; Denman et al., 2007; Meehl et al., 2007b; Le Quéré et al., 2009).

Studies with dynamic global vegetation models (DGVMs) have shown a considerable spread among models in the future trajectory of terrestrial biosphere carbon balance when forced with identical output fields from climate models (Cramer et al., 2001; Sitch et al., 2008). Studies in which a single DGVM is forced with data from an ensemble of GCMs likewise show a considerable spread in carbon balance, in this case stemming from differences in the climate simulated by different GCMs under the same CO_2 emission scenarios (Berthelot et al., 2005; Schaphoff et al., 2006). The spread among models – either DGVMs or the GCMs used to force them – may often be traced to contrasting simulated dynamics in a few specific regions, such as the Amazon Basin, where vegetation dieback and associated depletion of ecosystem carbon pools (Cox et al., 2000; Malhi et al., 2009) is simulated by some model combinations, but not by others (Berthelot et al., 2005; Schaphoff et al., 2006; Sitch et al., 2008). The impacts may be particularly dramatic when feedbacks of vegetation changes to the atmosphere through the carbon and hydrological cycles are accounted for by coupling the models to each other, simulated climate forcing the evolution of vegetation patterns and carbon pools, and vice-versa. In short, the available evidence suggests that the uncertainties induced by knowledge- and data gaps on both climate sensitivity (as encapsulated by different GCMs) and carbon cycle response (as encapsulated by different DGVMs) are large and of similar importance in terms of the limitations they impose on our current ability to project changes in the global climate.

While studies have demonstrated and quantified the uncertainty in the evolution of global terrestrial carbon balance over the coming century stemming from differences

BGD
9, 13685–13712, 2012

among GCMs (Berthelot et al., 2005; Schaphoff et al., 2006; Morales et al., 2007) the model characteristics and simulated mechanisms underlying this uncertainty have not been systematically analysed. In this paper, we employ a statistical emulator of a global terrestrial carbon cycle model (DGVM) as a tool to characterize GCM-based uncertainty in projected 21st century ecosystem-atmosphere carbon exchange, identifying major model characteristics underlying such uncertainty, and suggesting priorities for the further development and improvement of the GCMs.

2 Method and materials

2.1 Carbon cycle model

LPJ-GUESS is an individual-based, globally-applicable model of vegetation dynamics and biogeochemistry. It combines features of the Lund-Potsdam-Jena (LPJ) DGVM (Sitch et al., 2003; Gerten et al., 2004) with a more detailed treatment of plant resource competition and demography based on simulated interactions of plant individuals co-occurring in patches (Smith et al., 2001). Vegetation is represented by a mixture of plant functional types (PFTs, 11 in this study), differentiated by bioclimatic limits, growth form, phenology, photosynthetic pathway (C_3 or C_4) and life history strategy. LPJ-GUESS has been evaluated extensively and exhibits comparable skill to other approaches and models in reproducing observed temporal and spatial variation in large-scale vegetation patterns and ecosystem-atmosphere carbon exchange (Piao et al., 2012). Simulated carbon and evaporative fluxes have been compared to ecosystem flux measurements (Morales et al., 2005; Wramneby et al., 2008), forest inventory data and site-based measurements of NPP, leaf area index and biomass, spanning many of the world's biomes (Hickler et al., 2006; Zaehle et al., 2006; Smith et al., 2008, 2011; Tang et al., 2010, 2012). See Smith et al. (2001) for a detailed description of the model. The version used in this study includes the updates detailed in Hickler et al. (2012), and the same PFT set and configuration as described in Ahlström et al. (2012a).

BGD
9, 13685–13712, 2012

Our analysis was based on the simulated ecosystem carbon fluxes output by LPJ-GUESS, specifically gross primary production (GPP, i.e. the annual sum of canopy-level net photosynthesis for the vegetation in a grid cell), net primary production (NPP, i.e. GPP minus autotrophic (plant) respiration), ecosystem respiration (Er, i.e. the sum of, autotrophic and heterotrophic respiration), and biomass burning through wildfires (Fire). Net Biome Production (NBP) is the small difference between GPP and the release fluxes, Er and Fire. The total terrestrial carbon pool (Cpool) is the sum of the carbon residing in standing biomass and the organic layers of the soil. The cumulative sum of NBP over time is analogous to the change in Cpool.

2.2 Climate data

The LPJ-GUESS simulations were initialised with data from the CRU TS3.0 observed climate database (Mitchell and Jones, 2005) covering the period 1901–2000. From 2001, we forced LPJ-GUESS with simulations by four different GCMs, each with three atmospheric [CO_2] pathways based on the SRES emission scenarios (A2, A1B, B1) (Nakicenovic et al., 2000), giving in total twelve simulations. The data were obtained from the World Climate Research Programme's (WCRP) Coupled Model Intercomparison Project phase 3 (CMIP3) multi-model dataset (Meehl et al., 2007a). Four representative GCMs were chosen: CCSM3 (Collins et al., 2006), UKMO-HadCM3 (Gordon et al., 2000), IPSL-CM4 (Marti et al., 2005) and ECHAM5/MPI-OM (Roeckner et al., 2003). Further details of the simulation set up and forcing are provided in the Supplement, Text S1.

2.3 SVD analysis

We focused on sea-surface temperature (SSTs) as an overall indicator of those aspects of GCM-simulated climate of importance in terms of impacts on global ecosystem carbon balance. We characterized the relationship between SST patterns from a given GCM and NPP simulated by LPJ-GUESS when forced by that GCM by performing

BGD
9, 13685–13712, 2012

a Singular Value Decomposition (SVD) analysis of the global SST field. SVD is closely related to Empirical Orthogonal Functions (EOF) (also known as Principal Component Analysis or simply PCA, although definitions may sometimes vary). Both methods have been used to analyse spatial and temporal patterns of geophysical fields (e.g. Wallace et al., 1993; Uvo et al., 1998; Quadrelli and Wallace, 2004). The method can be used to decompose a dataset that varies in space and time into modes of spatial loading patterns, time series and singular values, where the modes are ordered so they explain a decreasing portion of variability in the original data sets (see, e.g. Bretherton et al. (1992) for a detailed description). The original data or subsets of it (e.g. the first three modes) can be recreated by combining the three products. The SVD time series (analogous to expansion coefficients, principal component time series or simply principal components) are vectors of the same length as the original data (here 80 yr). They are orthogonal (uncorrelated) and represent modes of variability, and often but not always correspond to different physical processes underlying the original data.

We applied SVD on the correlation matrix of the annual SST field of the SRES A2 simulations for each of the four GCMs presented above. Due to corrections (see text S1 in Appendix) of the variability and trend applied to the climate data between 2001 and 2020, we confined the SVD analysis to data from the period 2020–2099. For the three first SVD modes, we calculated the correlation between the resultant time series and to both the original SSTs and the simulated NPP in every gridcell (only first and second modes are presented in this paper). The resulting spatial pattern of correlations between SVD time series and original simulated SST shows how much the variability of the original simulated SST is related to the variability described by the specific SVD mode. On the other hand, the pattern of correlations between the SVD time series and the NPP illustrates the impact of SST variability in each mode on NPP over different regions. The statistical significance of the calculated correlations was tested using a bootstrap technique with 500 repetitions (Wilks, 2006).

The importance of each SVD mode was characterized as the squared covariance fraction (SCF), which corresponds to the fraction of the total SST variation explained

BGD
9, 13685–13712, 2012

by a given mode:

$$\mathrm{SCF} = \frac{l_i^2}{\sum l_i^2} \quad (1)$$

Where l_i is the i-th singular value, and SCF_i is the squared covariance fraction for the i-th mode. The analysis was repeated for NBP, and for precipitation and temperature to better understand the underlying driver of the resulting NPP and NBP patterns.

The global mean warming is well separated from variability not directly due to increased radiative forcing in the SSTs of the SRES A2 simulations. However, it is not always well separated in the SSTs of the lower emission scenarios, A1B and B1. Therefore, to be able to compare the α values from the replacement carbon cycle model (see next section) with a scenario-independent measure of SST variability we calculated the global average standard deviation of all the detrended SST time series. For every gridcell time series we removed the 2015–2085 trend (based on a 30-yr moving average of the global SST time series) using linear regression. Then we computed the standard deviation over the period 2015 through 2085 in every gridcell and averaged them globally, resulting in a single average value of the SST variability of each GCM simulation used except for CCSM3-B1 (SSTs for the latter were not available in the CMIP3 database).

2.4 Partitioning uncertainty in future carbon balance

A replacement model statistically emulating LPJ-GUESS was defined as a tool to enable uncertainty propagating from the four GCMs investigated to be extrapolated to a wider "space" of GCM behaviour by deterministic parameter resampling. Simple polynomials were fitted to global sums of GPP, Er, Fire and Cpool simulated by LPJ-GUESS under GCM forcing, with global average land temperature and atmospheric [CO_2] as the predictor variables. For GPP (in PgC), the resultant function has the form:

$$\mathrm{GPP}_t = \beta_1 + \beta_2 T_t + \beta_3 T_t^2 + \beta_4 \mathrm{CO}_{2_t} + \beta_5 \mathrm{CO}_{2_t}^2 + \beta_6 \mathrm{Cpool}_t + \beta_7 \mathrm{Cpool}_t^2 + \alpha \quad (2)$$

BGD
9, 13685–13712, 2012

Where t indicates the time step in years, β are the estimated parameters (Table A1), T (°C) is the global land temperature and Cpool (PgC) is the total terrestrial carbon pool from Eq. (4). The last term in the equation, α, is a simulation-specific parameter (PgC) that is allowed to vary between the 12 simulations used for the calibration. It represents factors influencing GPP not captured by land temperature and [CO_2], e.g. regional patterns of temperature, variability and variables not included in the replacement model forcing, such as precipitation and shortwave radiation. α was set to zero during the historical period (1901–2000), it was then linearly interpolated until 2020, similar to the forcing climate data. After 2020 it is held constant until the end of each simulation.

Equation (3) describes the sum of the global carbon fluxes from ecosystem respiration and wild fires (PgC) as a function of global land temperature, GPP from Eq. (2) and Cpool from Eq. (4).

$$\mathrm{Er} + \mathrm{Fire}_t = \beta_8 + \beta_9 T_t + \beta_{10} T_t^2 + \beta_{11} \mathrm{GPP}_t + \beta_{12} \mathrm{Cpool}_t \quad (3)$$

In Eq. (4) the total carbon pool of the next time step (yr) is calculated as the present year's carbon pool plus the current year's net carbon exchange, NBP.

$$\mathrm{Cpool}_{t+1} = \mathrm{Cpool}_t + \mathrm{GPP}_t - (\mathrm{Er} + \mathrm{Fire})_t \quad (4)$$

All parameters β_{1-12} (Eqs. 2 and 3) were estimated simultaneously by minimizing the sum of the square of the errors (SSE) between the resulting GPP, Er + Fire, Cpool and the corresponding LPJ-GUESS simulation results; see Table S1 for parameter values.

To better separate the CO_2 signal from the temperature signal we used the full length of the climate data series, including the "stabilization" period after 2100 when [CO_2] were held constant, but temperature continued to evolve. The length of the stabilization period varied between the datasets of the A1B scenario, resulting in a slightly uneven weighting of the four GCMs.

The replacement model uses the area-weighted average of land temperatures, T, as a predictor variable. However, land temperatures may evolve at a different rate than the global mean surface temperature – which also accounts for temperatures over

BGD
9, 13685–13712, 2012

the oceans, inland water bodies and ice-sheets – in GCM simulations. We calculated a factor, γ, that expresses the degree of amplification in the temperature trend over land relative to the global mean surface temperatures, with 1961–1990 mean temperatures as a baseline:

$$\Delta LT_t = \gamma \times \Delta GT_t + \varepsilon_t \quad (5)$$

Where ΔLT_t is the mean land temperature change by year t compared with the 1961–1990 average. ΔGT_t is the global mean surface temperature change compared with the 1961–1990 average. Now land temperature T in the replacement model (Eqs. 2 and 3) can be calculated from global mean surface temperature following:

$$T_t = \overline{T}_{61-90} + \gamma \times \Delta GT_t \quad (6)$$

Where $\overline{T}_{61-90}$ represents the average 1961–1990 land temperature in the CRU dataset.

To partition the variation in future terrestrial carbon balance suggested by our simulations to underlying factors in the GCMs and [CO_2] pathways providing the forcing, we adopted a permutation approach, using the statistical replacement model (Eqs. 2–4) to generate 192 synthetic time series, corresponding to all possible combinations of the main independent forcing factors encompassed by our analysis, namely the three [CO_2] pathways, the four corresponding global temperature change (ΔGT) (one simulated by each GCM), four GCM-average values of the simulation-specific parameter α in Eq. (2), and four GCM-average values of the land-to-global warming ratio, γ, from Eq. (6). For each combination we estimated the 2000–2100 carbon balance trajectory using the replacement model (Eqs. 2–4). We thus created an ensemble of 60 "artificial" GCMs with different characteristics, in addition to the original four, combining each with one of the three [CO_2] pathways, to produce a suite of 192 plausible carbon balance trajectories.

To attribute variation in the resultant carbon balance time series to underlying forcing factors, we performed analysis of variance (ANOVA; Draper and Smith 1998) with α,

BGD
9, 13685–13712, 2012

γ, and [CO_2] pathway (A2, A1B, B1) as independent factors. The ANOVA separates the total sum of squares in the simulated change in total carbon stock from 2000–2099 into sum of squares due to each of the three factors above and a residual term that contains effects due to interactions between factors and an unexplained component, such as temperature. Since the temperature depends on the specific CO_2 scenario, it is non-trivial to quantify the effect of different temperatures, forcing us to limit the ANOVA to the three factors α, γ, and CO_2.

3 Results

3.1 Carbon cycle simulations

The LPJ-GUESS simulations forced by different GCMs and [CO_2] pathways result in wide range of trajectories for Cpool (Fig. 1). Simulations forced by climate data from the same GCM under different CO_2 emission scenarios tend to cluster, indicating that differences between GCMs exert a stronger control on Cpool than [CO_2] pathways. By 2099, the largest difference between the simulations, 247 Pg C, is found between the simulation forced by CCSM3 under the A1B and HadCM3 under the B1 emissions scenario. Regardless of emissions scenario, the largest contrast is found between the simulations forced by CCSM3 and HadCM3.

3.2 GCM climate-carbon cycle relationships

The SVD time series of the first two modes, the SST spatial correlation patterns and the NPP correlation patterns for the time period 2020–2099 are illustrated in Fig. 2. The first mode of variability is closely related to the global temperature trend and variability as indicated by the overall strong correlation over all the world's oceans (Fig. 2a, column). The variability and trend of the SVD time series of the first mode show similarities with the standardized global land temperatures (Fig. 2e). The Squared Covariance Fraction (SCF) differs between the GCMs. A high SCF in the first mode implies a relatively

BGD
9, 13685–13712, 2012

globally uniform pattern of variability (CCSM3) while a lower amount of SCF in the first SVD mode (HadCM3 and ECHAM5) implies a larger proportion of local variability of the total global SST variability.

The second mode of variability (Fig. 2b) explains around an order of magnitude less of the total variance of the simulated SSTs for all four GCMs, and is generally characterized by El Niño-Southern Oscillation (ENSO) like patterns. The ENSO patterns are more prominent in the SSTs of ECHAM5 and HadCM3 compared with the other GCMs, while for CM4 they are more pronounced in the third mode (not shown here) than in the second mode, indicating that other variation, not primarily associated with ENSO, is influencing the second mode of variability for this GCM. Time series for the first two modes (Fig. 2e) show, as expected, a uniform up-going trend in the first mode consistent with global warming response to rising greenhouse gas concentrations, while the second mode exhibits continuous fluctuations with no obvious trends for any of the models.

The third and fourth columns (Fig. 2c, d) show the correlation between the same SVD time series and simulated NPP. Global temperature increase, together with the co-varying [CO_2] (closely related to the first mode of variability of the simulated SSTs) are associated with increasing NPP in most areas, except in some tropical regions, where a negative correlation is seen. The tropical NPP decline is most pronounced in the simulation forced by HadCM3, where parts of tropical South America and Western North Africa see a decreased NPP resulting from the negative impacts of decreased precipitation and/or increased evapotranspiration under higher temperatures on plant water relations (Figs. S1 and S2).

The correlation patterns between the second SVD mode and NPP (Fig. 2d) illustrate the impact of ENSO-related regional climate patterns on land ecosystems, particularly water relations. For HadCM3, ENSO leads to pronounced decrease of NPP in the tropics and Australia and increased NPP in Western North America and the Middle East. In ECHAM5 the negative impact is more pronounced in Australia but less pronounced in the tropics. The regions that show increased NPP are similar for both models. The

BGD
9, 13685–13712, 2012

direct cause of the NPP declines in HadCM3 and ECHAM5 is decreased precipitation and increased temperature (Figs. S1 and S2).

CCSM3 shows a similar but considerably weaker correlation pattern to ECHAM5, while CM4 shows no strong patterns, probably because ENSO dynamics for that GCM are expressed mainly in the third mode. Correlation patterns between SST modes and NBP, shown in Fig. S3, are generally reminiscent of the results for NPP, reflecting the driving role of vegetation productivity in the carbon cycling of ecosystems as a whole.

3.3 GCM-dependent uncertainty in carbon balance

GCM-simulated global mean land temperature and the [CO_2] pathway of the underlying emission scenario explain part, but not all, of the variation between simulations in the evolution of the terrestrial carbon pool over the 21st century, as simulated by LPJ-GUESS. The remaining, unexplained, source of variation, signified by α in Eq. (2), encapsulates the regional patterns of carbon balance and their evolution over time, specific to each GCM × emissions scenario combination (Fig. 3). The displacement between the black (simulation-specific fit for α) and grey (α set to the average of the twelve simulation-specific values) curve in each frame of Fig. 3 represents the effect of this unexplained variation in each individual simulation.

The SVD analysis reveals differences in the impact on simulated NPP and NBP, induced by differences among GCMs related to SST variability and associated weather patterns (see Fig. 2). We found a strong relationship between α and global SST variability (Fig. 4). The α values cluster according to GCMs and not according to CO_2 emission scenarios, signifying a strong GCM-dependence for this parameter. The CCSM3 simulations show the highest uptake of carbon (Fig. 1). The corresponding α values are also the least negative (Fig. 4). The CM4 simulations group in the middle, and show a decrease of about 7 PgC in GPP per year compared to the historical simulation. ECHAM5 and HadCM3 show larger SST variability compared to CM4 and CCSM3, and the simulations forced with these models also have the most negative α values of

BGD
9, 13685–13712, 2012

all the simulations. All simulations have an α value lower than the historical simulation (which is 0).

3.4 Global versus land temperature

The ratio of land to global warming γ varied from 1.26 to 1.46 between the 12 datasets for 2001–2009 (Fig. 5). CCSM3 shows the lowest γ (least amplification of warming over land) for all scenarios while HadCM3 shows the highest γ for all scenarios. A single GCM-specific factor seems to be enough to explain most variation in γ as long as the climate forcing is increasing. In the longest dataset used here, the CM4 A1B, top, middle column in Fig. 5, it is evident that the discrepancy between the global and land temperatures are becoming smaller at the end of the simulation where [CO_2] has been held constant since 2100. The range in A2 global temperature (2095–2099) is 0.27 °C, which more than doubles when looking at the land temperature (0.57 °C). The global average temperature change, ΔGT, (2095–2099) of the HadCM3 model's A2 scenario is the lowest of the four (3.9 °C), while the land temperature, ΔLT, for the same period, GCM and scenario is the highest of the four (5.7 °C).

4 Partitioning uncertainty in carbon balance

Using the replacement carbon balance model to sample across 192 combinations of GCM- and scenario characteristics (see Methods), we came up with the distribution of carbon balance trajectories shown in Fig. 6. For this ensemble of [CO_2] pathways and GCMs, and given the carbon cycle representation in LPJ-GUESS, total terrestrial carbon stocks may increase or decrease by the end of the 21st century, but are more likely to increase. Note that the percentiles and the medians shown in Fig. 6 are partly a result of the sampling of sampling. It is apparent that much of the uncertainty represented by the spread among trajectories propagates from different characteristics and behaviour of GCMs. According to the ANOVA analysis, 91 % of the variability among

BGD
9, 13685–13712, 2012

trajectories could be explained by the two GCM-specific factors α (87 %) and γ (5 %). The choice of CO_2 emission scenario explains just 2 % of the variation, while 7 % remains unexplained (Fig. 6).

5 Discussion

The LPJ-GUESS simulations forced by the ensemble of GCMs and CO_2 emission scenarios chosen for this study result in a considerable spread in the future evolution of carbon balance. Our results demonstrate that the majority of this spread can be traced to a GCM-specific parameter (α) closely related to global SST variability.

As seen in Fig. 4, all the GCMs show a negative α value (α was set to 0 for CRU). One interpretation could be that all GCMs show unrealistically large climate variability or other climate characteristics that negatively influence GPP. However, the offset of the α values in comparison to CRU can also be explained by the offset between the GCMs and CRU as a result of different trends since the 1961–1990 climatology. Additionally, as a result of station data limitations, around 13 % of the CRU gridcells used in this study show at least one consecutive 10-yr period with no interannual variability (see Fig. S4). Therefore it is difficult to draw conclusions about which α value is the most realistic, or if all GCMs give too low α values.

Because our results are based on four GCMs we do not know how much of the spread between all the CMIP3 GCMs we have captured. If the relationships found apply to other GCMs (or later versions of the four we have explicitly considered) remains to be tested. Still, our results provide some quantification of GCM discrepancies and their impact on carbon balance as simulated by LPJ-GUESS.

When applying the replacement model with combinations of the GCM specific parameters and variables we assume that they are independent. When averaging γ and α across GCMs ($n = 4$), they show no significant correlation ($r = -0.93$, n.s.) but when we use all simulations ($n = 12$), they show a significant correlation ($r = -0.92$, $P < 0.00005$). However, the correlation could be a coincidence as a result of the selec-

BGD
9, 13685–13712, 2012

tion of GCMs. Amongst many factors and processes it is plausible that GCM differences in, e.g. energy balance, the partitioning of latent and sensible heat can influence both α and γ. Other possible differences between GCMs, such as differences in ocean overturning or the melting of sea ice affecting ocean warming, potentially influencing γ are likely to have smaller effect on α.

ENSO is the dominant determinant of global precipitation variability (Dai et al., 1997). A prominent effect of warm ENSO events is negative precipitation anomalies in large parts of the tropics, but also significant precipitation anomalies in other regions can be traced back to ENSO (Dai and Wigley, 2000). Patterns of correlation between pacific SST variability and precipitation reminiscent of ENSO have been found to emerge in GCM simulations. The SVD analysis of sea surface temperatures presented here reveals carbon cycle patterns similar to those found by Dai (2006) when analysing rainfall patterns and tropical SST variability in HadCM3, ECHAM5 and CCSM3 amongst other GCMs. Although the "strength" of representation of ENSO differs between GCMs, a strong dependency of low latitude precipitation and tropical SST variability is typically simulated on interannual and longer timescales (Dai, 2006).

The effects of droughts on carbon fluxes in the Amazon basin have been debated. Satellite-based studies have reported a "green up" in the Amazon rainforest during dry conditions as a result of increased incoming solar radiation when cloud cover decreases (Huete et al., 2006; Saleska et al., 2007). However, field studies have reported increased tree mortality and carbon loss during severe droughts (Nepstad et al., 2007; Brando et al., 2008; Phillips et al., 2009), resulting from decreased plant available water and/or heat stress (Toomey et al., 2011). Recent studies employing a satellite based model and a DGVM have suggested a strong NPP dependency on plant available water and susceptibility to droughts in tropical regions over the last decade (Zhao and Running, 2010; Ahlström et al., 2012b). Impacts of droughts on tropical vegetation has been demonstrated to be a major uncertainty in carbon balance in modelling studies applying several GCMs to force ecosystem models (Berthelot et al., 2005; Schaphoff et al., 2006; Ahlström et al., 2012b). The negative NPP and NBP anomalies found have

BGD
9, 13685–13712, 2012

either been explained by decreased precipitation (Schaphoff et al., 2006) or increased temperatures (Berthelot et al., 2005), leading to increased plant respiration and/or exerting an indirect negative effect on plant available water by increasing the atmospheric demand for water vapour. The results presented here concur with previous studies in attributing the majority of the uncertainties in future global terrestrial carbon cycle to decreased plant available water mainly in the tropics, a result of re-occurring droughts, induced by SST variations accompanied by more static regional differences in future climatology.

6 Conclusions

Our results point to a marked dependency of the future development of global terrestrial ecosystem carbon balance on climate characteristics, particularly SST variability and its impact on weather patterns, which differ among GCMs. A further GCM characteristic, the degree of enhancement of warming over land relative to global warming generally, accounts for the second largest portion of uncertainty in carbon balance response. Uncertainty stemming from the choice of CO_2 emission scenario is much less marked. Finally, our results suggest that improved ENSO representation and low latitude precipitation patterns are important to narrow the uncertainties in future climate change projections using ESMs or uncoupled DGVMs forced by GCMs.

Supplementary material related to this article is available online at: http://www.biogeosciences-discuss.net/9/13685/2012/bgd-9-13685-2012-supplement.pdf.

Acknowledgements. This study was funded by the Foundation for Strategic Environment Research (Mistra) through the Mistra-SWECIA programme. The study is a contribution to the Lund University Strategic Research Areas Modelling the Regional and Global Earth System

BGD
9, 13685–13712, 2012

(MERGE) and Biodiversity and Ecosystem Services in a Changing Climate (BECC). We acknowledge the global modelling groups, the Program for Climate Model Diagnosis and Intercomparison (PCMDI) and the WCRP's Working Group on Coupled Modelling (WGCM) for their roles in making available the WCRP CMIP3 multi-model dataset. Support of this dataset is provided by the Office of Science, US Department of Energy.

References

Ahlström, A., Miller, P. A., and Smith, B.: Too early to infer a global NPP decline since 2000, Geophys. Res. Lett., 39, L15403, doi:10.1029/2012gl052336, 2012.

Ahlström, A., Schurgers, G., Arneth, A., and Smith, B.: Robustness and uncertainty in terrestrial ecosystem carbon response to CMIP5 climate change projections, Environ. Res. Lett., accepted, 2012.

Berthelot, M., Friedlingstein, P., Ciais, P., Dufresne, J.-L., and Monfray, P.: How uncertainties in future climate change predictions translate into future terrestrial carbon fluxes, Glob. Change Biol., 11, 959–970, doi:10.1111/j.1365-2486.2005.00957.x, 2005.

Brando, P. M., Nepstad, D. C., Davidson, E. A., Trumbore, S. E., Ray, D., and Camargo, P.: Drought effects on litterfall, wood production and belowground carbon cycling in an Amazon forest: results of a throughfall reduction experiment, Philos. T. R. Soc. B, 363, 1839–1848, doi:10.1098/rstb.2007.0031, 2008.

Bretherton, C. S., Smith, C., and Wallace, J. M.: An intercomparison of methods for finding coupled patterns in climate data, J. Climate, 5, 541–560, doi:10.1175/1520-0442(1992)005<0541:aiomff>2.0.co;2, 1992.

Canadell, J. G., Le Quéré, C., Raupach, M. R., Field, C. B., Buitenhuis, E. T., Ciais, P., Conway, T. J., Gillett, N. P., Houghton, R. A., and Marland, G.: Contributions to accelerating atmospheric CO_2 growth from economic activity, carbon intensity, and efficiency of natural sinks, P. Natl. Acad. Sci. USA, 104, 18866–18870, doi:10.1073/pnas.0702737104, 2007.

Collins, W. D., Bitz, C. M., Blackmon, M. L., Bonan, G. B., Bretherton, C. S., Carton, J. A., Chang, P., Doney, S. C., Hack, J. J., Henderson, T. B., Kiehl, J. T., Large, W. G., McKenna, D. S., Santer, B. D., and Smith, R. D.: The community climate system model version 3 (CCSM3), J. Climate, 19, 2122–2143, doi:10.1175/jcli3761.1, 2006.

BGD
9, 13685–13712, 2012

Cramer, W., Bondeau, A., Woodward, F. I., Prentice, I. C., Betts, R. A., Brovkin, V., Cox, P. M., Fisher, V., Foley, J. A., Friend, A. D., Kucharik, C., Lomas, M. R., Ramankutty, N., Sitch, S., Smith, B., White, A., and Young-Molling, C.: Global response of terrestrial ecosystem structure and function to CO_2 and climate change: results from six dynamic global vegetation models, Glob. Change Biol., 7, 357–373, doi:10.1046/j.1365-2486.2001.00383.x, 2001.

Dai, A. and Wigley, T. M. L.: Global patterns of ENSO-induced precipitation, Geophys. Res. Lett., 27, 1283–1286, doi:10.1029/1999gl011140, 2000.

Dai, A., Fung, I. Y., and Del Genio, A. D.: Surface observed global land precipitation variations during 1900–88, J. Climate, 10, 2943–2962, doi:10.1175/1520-0442(1997)010<2943:soglpv>2.0.co;2, 1997.

Dai, A.: Precipitation characteristics in eighteen coupled climate models, J. Climate, 19, 4605–4630, doi:10.1175/jcli3884.1, 2006.

Denman, K. L., Brasseur, G., Chidthaisong, A., Ciais, P., Cox, P. M., Dickinson, R. E., Hauglustaine, D., Heinze, C., Holland, E., Jacob, D., Lohmann, U., Ramachandran, S., da Silva Dias, P. L., Wofsy, S. C., and Zhang, X.: Couplings between changes in the climate system and biogeochemistry, in: Climate Change 2007: The Physical Science Basis. Contribution of Working Group I to the Fourth Assessment Report of the Intergovernmental Panel on Climate Change, edited by: Solomon, S., Qin, D., Manning, M., Chen, Z., Marquis, M., Averyt, K. B., Tignor, M., and Miller, H. L., Cambridge University Press, Cambridge, UK and New York, NY, USA, 499–587, 2007.

Gerten, D., Schaphoff, S., Haberlandt, U., Lucht, W., and Sitch, S.: Terrestrial vegetation and water balance–hydrological evaluation of a dynamic global vegetation model, J. Hydrol., 286, 249–270, doi:10.1016/j.jhydrol.2003.09.029, 2004.

Gordon, C., Cooper, C., Senior, C. A., Banks, H., Gregory, J. M., Johns, T. C., Mitchell, J. F. B., and Wood, R. A.: The simulation of SST, sea ice extents and ocean heat transports in a version of the Hadley Centre coupled model without flux adjustments, Clim. Dynam., 16, 147–168, doi:10.1007/s003820050010, 2000.

Hickler, T., Prentice, I. C., Smith, B., Sykes, M. T., and Zaehle, S.: Implementing plant hydraulic architecture within the LPJ dynamic global vegetation model, Global Ecol. Biogeogr., 15, 567–577, doi:10.1111/j.1466-8238.2006.00254.x, 2006.

Hickler, T., Vohland, K., Feehan, J., Miller, P. A., Smith, B., Costa, L., Giesecke, T., Fronzek, S., Carter, T. R., Cramer, W., Kühn, I., and Sykes, M. T.: Projecting the future distribution of European potential natural vegetation zones with a generalized, tree species-based dynamic veg-

BGD
9, 13685–13712, 2012

etation model, Global Ecol. Biogeogr., 21, 50–63, doi:10.1111/j.1466-8238.2010.00613.x, 2012.
Huete, A. R., Didan, K., Shimabukuro, Y. E., Ratana, P., Saleska, S. R., Hutyra, L. R., Yang, W., Nemani, R. R., and Myneni, R.: Amazon rainforests green-up with sunlight in dry season, Geophys. Res. Lett., 33, L06405, doi:10.1029/2005gl025583, 2006.
Knutti, R., and Hegerl, G. C.: The equilibrium sensitivity of the Earth's temperature to radiation changes, Nat. Geosci., 1, 735–743, 2008.
Le Quéré, C., Raupach, M. R., Canadell, J. G., Marland, G., Bopp, L., Ciais, P., and Conway, T. J.: Trends in the sources and sinks of carbon dioxide, Nat. Geosci., 2, 831–836, doi:10.1038/ngeo689, 2009.
Marti, O., Braconnot, P., Bellier, J., Benshila, R., Bony, S., Brockmann, P., Cadule, P., Caubel, A., Denvil, S., Dufresne, J. L., Fairhead, L., Filiberti, M.-A., Fichefet, T., Foujols, M.-A., Friedlingstein, P., Grandpeix, J.-Y., Hourdin, F., Krinner, G., Lévy, C., Madec, G., Musat, I., De Noblet, N., Polcher, J., and Talandier, C.: The new IPSL Climate System Model: IPSL-CM4 , 1–86, 2005.
Meehl, G. A., Covey, C., Delworth, T., Latif, M., McAvaney, B., Mitchell, J. F. B., Stouffer, R. J., and Taylor, K. E.: The WCRP CMIP3 multimodel dataset: a new era in climate change research, B. Am. Meteorol. Soc., 88, 1383–1394, 2007a.
Meehl, G. A., Stocker, T., Collins, W., Friedlingstein, A., Gaye, A., Gregory, J., Kitoh, A., Knutti, R., Murphy, J., and Noda, A.: Global climate projections, in: Climate Change 2007: The Physical Science Basis. Contribution of Working Group 1 to the Fourth Assessment report of the Intergovernmental Panel on Climate Change, edited by: Solomon, S., Qin, D., Manning, M., Chen, Z., Marquis, M., Averyt, K., Tignor, M., and Miller, H., Cambridge University Press, Cambridge, United kingdom and New York, NY, US A., 2007b.
Morales, P., Sykes, M. T., Prentice, I. C., Smith, P., Smith, B., Bugmann, H., Zierl, B., Friedlingstein, P., Viovy, N., Sabaté, S., Sánchez, A., Pla, E., Gracia, C. A., Sitch, S., Arneth, A., and Ogee, J.: Comparing and evaluating process-based ecosystem model predictions of carbon and water fluxes in major European forest biomes, Glob. Change Biol., 11, 2211–2233, doi:10.1111/j.1365-2486.2005.01036.x, 2005.
Morales, P., Hickler, T., Rowell, D. P., Smith, B., and Sykes, M. T.: Changes in European ecosystem productivity and carbon balance driven by regional climate model output, Glob. Change Biol., 13, 108–122, doi:10.1111/j.1365-2486.2006.01289.x, 2007.

BGD
9, 13685–13712, 2012

Nakicenovic, N., Alcamo, J., Davis, G., de Vries, B., Fenhann, J., Gaffin, S., Gregory, K., Grubler, A., Jung, T. Y., Kram, T., La Rovere, E. L., Michaelis, L., Mori, S., Morita, T., Pepper, W., Pitcher, H. M., Price, L., Riahi, K., Roehrl, A., Rogner, H.-H., Sankovski, A., Schlesinger, M., Shukla, P., Smith, S. J., Swart, R., van Rooijen, S., Victor, N., and Dadi, Z.: IPCC Special Report on Emissions Scenarios: a special report of Working Group III of the Intergovernmental Panel on Climate Change, edited by: Nakicenovic, N. and Swart, R., Cambridge University Press, Cambridge, UK, 2000.

Nepstad, D. C., Tohver, I. M., Ray, D., Moutinho, P., and Cardinot, G.: Mortality of large trees and lianas following experimental drought in an Amazon forest, Ecology, 88, 2259–2269, doi:10.1890/06-1046.1, 2007.

Phillips, O. L., Aragão, L. E. O. C., Lewis, S. L., Fisher, J. B., Lloyd, J., López-González, G., Malhi, Y., Monteagudo, A., Peacock, J., Quesada, C. A., van der Heijden, G., Almeida, S., Amaral, I., Arroyo, L., Aymard, G., Baker, T. R., Bánki, O., Blanc, L., Bonal, D., Brando, P., Chave, J., de Oliveira, Á. C. A., Cardozo, N. D., Czimczik, C. I., Feldpausch, T. R., Freitas, M. A., Gloor, E., Higuchi, N., Jiménez, E., Lloyd, G., Meir, P., Mendoza, C., Morel, A., Neill, D. A., Nepstad, D., Patiño, S., Peñuela, M. C., Prieto, A., Ramírez, F., Schwarz, M., Silva, J., Silveira, M., Thomas, A. S., Steege, H. t., Stropp, J., Vásquez, R., Zelazowski, P., Dávila, E. A., Andelman, S., Andrade, A., Chao, K.-J., Erwin, T., Di Fiore, A., Honorio C, E., Keeling, H., Killeen, T. J., Laurance, W. F., Cruz, A. P., Pitman, N. C. A., Vargas, P. N., Ramírez-Angulo, H., Rudas, A., Salamão, R., Silva, N., Terborgh, J., and Torres-Lezama, A.: Drought sensitivity of the Amazon rainforest, Science, 323, 1344–1347, doi:10.1126/science.1164033, 2009.

Piao, S., Sitch, S., Ciais, P., Friedlingstein, P., Peylin, P., Wang, X., Ahlström, A., Alessandro, A., Canadell, J. G., Huntingford, C., Jung, M., Levis, S., Levy, P. E., Lomas, M. R., Luo, Y., Myneni, R. B., Poulter, B., Viovy, N., Zaehle, S., and Zeng, N.: Evaluation of terrestrial carbon cycle models for their sensitivity to climate changes and rising atmospheric CO_2 concentrations, Glob. Change Biol., submitted, 2012.

Quadrelli, R., and Wallace, J. M.: A simplified linear framework for interpreting patterns of Northern Hemisphere wintertime climate variability, J. Climate, 17, 3728–3744, doi:10.1175/1520-0442(2004)017<3728:aslffi>2.0.co;2, 2004.

Roeckner, E., Bäuml, G., Bonaventura, L., Brokopf, R., Esch, M., Giorgetta, M., Hagemann, S., Kirchner, I., Kornblueh, L., Manzini, E., Rhodin, A., Schlese, U., Schulzweida, U., and Tomp-

BGD
9, 13685–13712, 2012

kins, A.: The atmospheric general circulation model ECHAM5, Part I: Model description, 127, 2003.
Saleska, S. R., Didan, K., Huete, A. R., and da Rocha, H. R.: Amazon forests green-up during 2005 drought, Science, 318, 612, doi:10.1126/science.1146663, 2007.
Schaphoff, S., Lucht, W., Gerten, D., Sitch, S., Cramer, W., and Prentice, I.: Terrestrial biosphere carbon storage under alternative climate projections, Climatic Change, 74, 97–122, doi:10.1007/s10584-005-9002-5, 2006.
Sitch, S., Smith, B., Prentice, I. C., Arneth, A., Bondeau, A., Cramer, W., Kaplan, J. O., Levis, S., Lucht, W., Sykes, M. T., Thonicke, K., and Venevsky, S.: Evaluation of ecosystem dynamics, plant geography and terrestrial carbon cycling in the LPJ dynamic global vegetation model, Glob. Change Biol., 9, 161–185, doi:10.1046/j.1365-2486.2003.00569.x, 2003.
Sitch, S., Huntingford, C., Gedney, N., Levy, P. E., Lomas, M., Piao, S. L., Betts, R., Ciais, P., Cox, P., Friedlingstein, P., Jones, C. D., Prentice, I. C., and Woodward, F. I.: Evaluation of the terrestrial carbon cycle, future plant geography and climate-carbon cycle feedbacks using five dynamic global vegetation models (DGVMs), Glob. Change Biol., 14, 2015–2039, doi:10.1111/j.1365-2486.2008.01626.x, 2008.
Smith, B., Prentice, I. C., and Sykes, M. T.: Representation of vegetation dynamics in the modelling of terrestrial ecosystems: comparing two contrasting approaches within European climate space, Global Ecol. Biogeogr., 10, 621–637, doi:10.1046/j.1466-822X.2001.t01-1-00256.x, 2001.
Smith, B., Knorr, W., Widlowski, J.-L., Pinty, B., and Gobron, N.: Combining remote sensing data with process modelling to monitor boreal conifer forest carbon balances, Forest Ecol. Manag., 255, 3985–3994, doi:10.1016/j.foreco.2008.03.056, 2008.
Smith, B., Samuelsson, P., Wramneby, A., and Rummukainen, M.: A model of the coupled dynamics of climate, vegetation and terrestrial ecosystem biogeochemistry for regional applications, Tellus A, 63, 87–106, doi:10.1111/j.1600-0870.2010.00477.x, 2011.
Tang, G., Beckage, B., Smith, B., and Miller, P. A.: Estimating potential forest NPP, biomass and their climatic sensitivity in New England using a dynamic ecosystem model, Ecosphere, 1, 18, doi:10.1890/es10-00087.1, 2010.
Tang, G., Beckage, B., and Smith, B.: The potential transient dynamics of forests in New England under historical and projected future climate change, Climatic Change, 1–21, doi:10.1007/s10584-012-0404-x, 2012.

BGD
9, 13685–13712, 2012

Toomey, M., Roberts, D. A., Still, C., Goulden, M. L., and McFadden, J. P.: Remotely sensed heat anomalies linked with Amazonian forest biomass declines, Geophys. Res. Lett., 38, L19704, doi:10.1029/2011gl049041, 2011.

Uvo, C. B., Repelli, C. A., Zebiak, S. E., and Kushnir, Y.: The relationships between Tropical Pacific and Atlantic SST and Northeast Brazil monthly precipitation, J. Climate, 11, 551–562, doi:10.1175/1520-0442(1998)011<0551:trbtpa>2.0.co;2, 1998.

Wallace, J. M., Zhang, Y., and Lau, K.-H.: Structure and seasonality of interannual and interdecadal variability of the geopotential height and temperature fields in the Northern Hemisphere troposphere, J. Climate, 6, 2063–2082, doi:10.1175/1520-0442(1993)006<2063:sasoia>2.0.co;2, 1993.

Wilks, D. S.: Statistical Methods in the Atmospheric Sciences, 2nd edn., Academic Press, 627 pp., 2006.

Wramneby, A., Smith, B., Zaehle, S., and Sykes, M. T.: Parameter uncertainties in the modelling of vegetation dynamics – effects on tree community structure and ecosystem functioning in European forest biomes, Ecol. Model., 216, 277–290, doi:10.1016/j.ecolmodel.2008.04.013, 2008.

Zaehle, S., Sitch, S., Prentice, I. C., Liski, J., Cramer, W., Erhard, M., Hickler, T., and Smith, B.: The importance of age-related decline in forest NPP for modeling regional carbon balances, Ecol. Appl., 16, 1555–1574, 2006.

Zhao, M. and Running, S. W.: Drought-induced reduction in global terrestrial net primary production from 2000 through 2009, Science, 329, 940–943, doi:10.1126/science.1192666, 2010.

BGD
9, 13685–13712, 2012

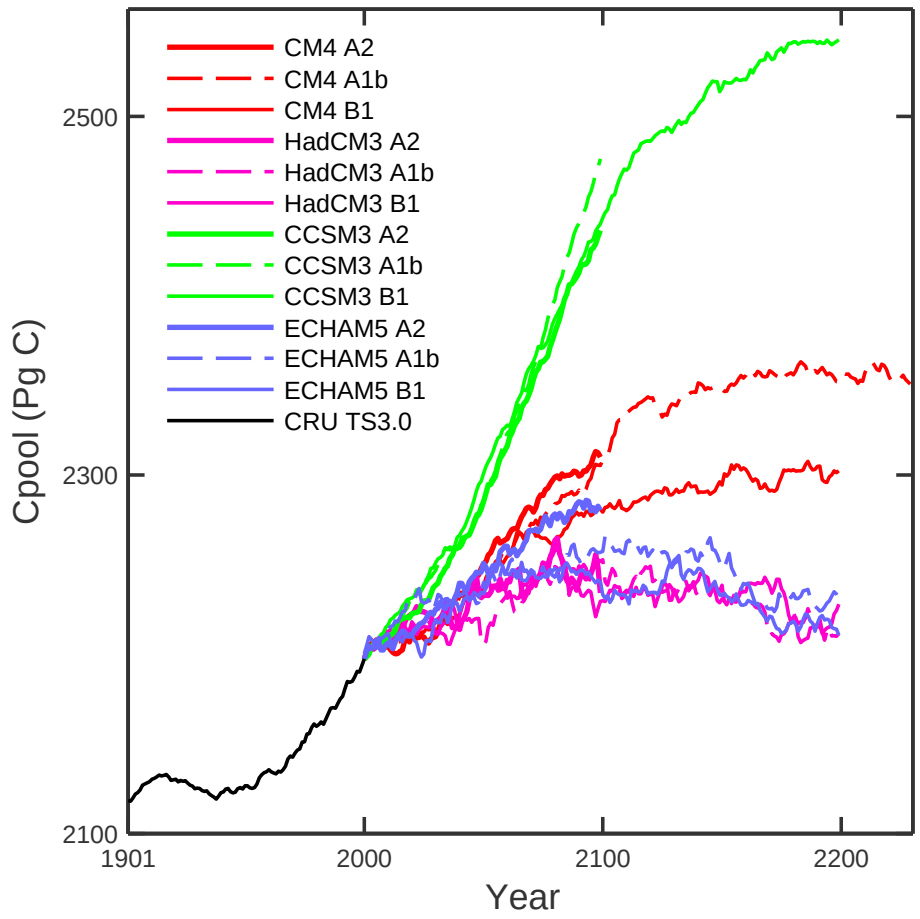

Fig. 1. Evolution of the global terrestrial ecosystem carbon pool (Cpool) under twelve future scenario simulations with LPJ-GUESS.

BGD
9, 13685–13712, 2012

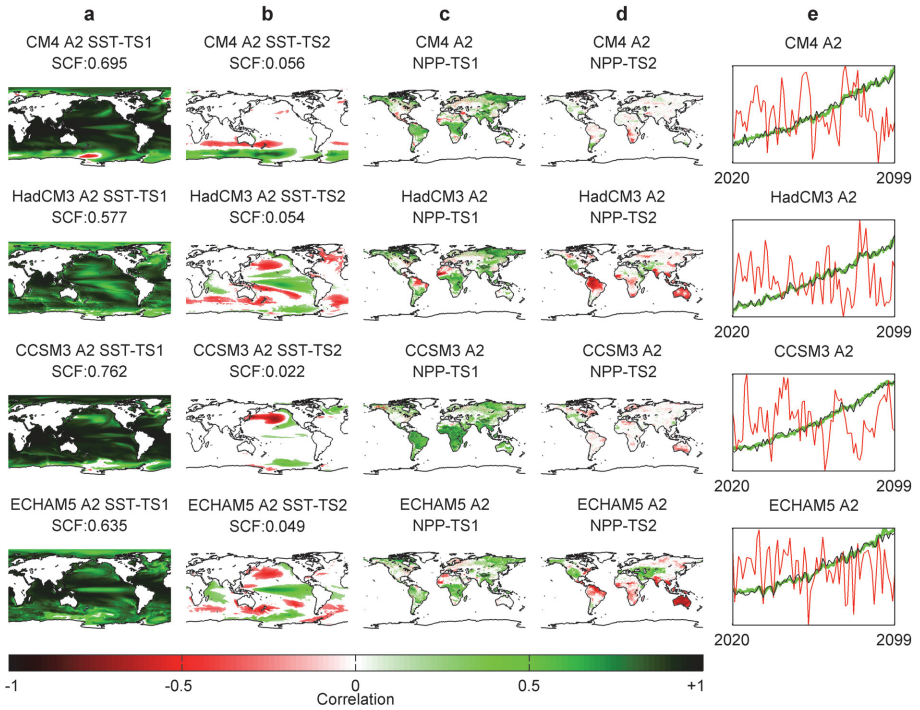

Fig. 2. Spatial patterns of correlation (Pearson *r*) between the first two SVD modes of GCM-simulated SST under the A2 scenario and (**a** and **b**) the original simulated SST, and (**c** and **d**) NPP by LPJ-GUESS. The correlations presented in colours are all statistically significant at 5 % level. **(e)** standardized time series of the first SVD mode (green), second SVD mode (red) and global land temperature (black).

BGD
9, 13685–13712, 2012

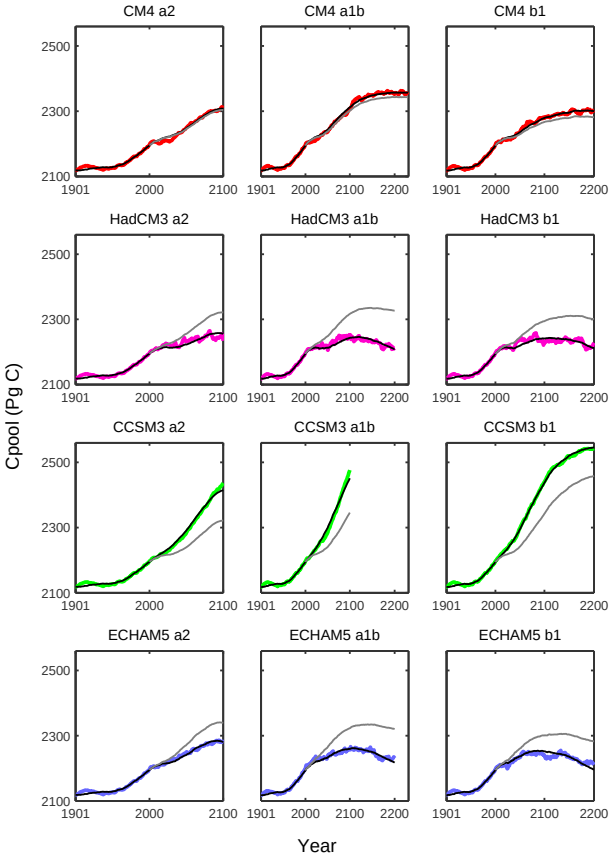

Fig. 3. Global terrestrial ecosystem carbon pool (Cpool) as simulated by LPJ-GUESS (colours) and the dynamic replacement model with average α (grey) or simulation-specific fit for α (black).

BGD
9, 13685–13712, 2012

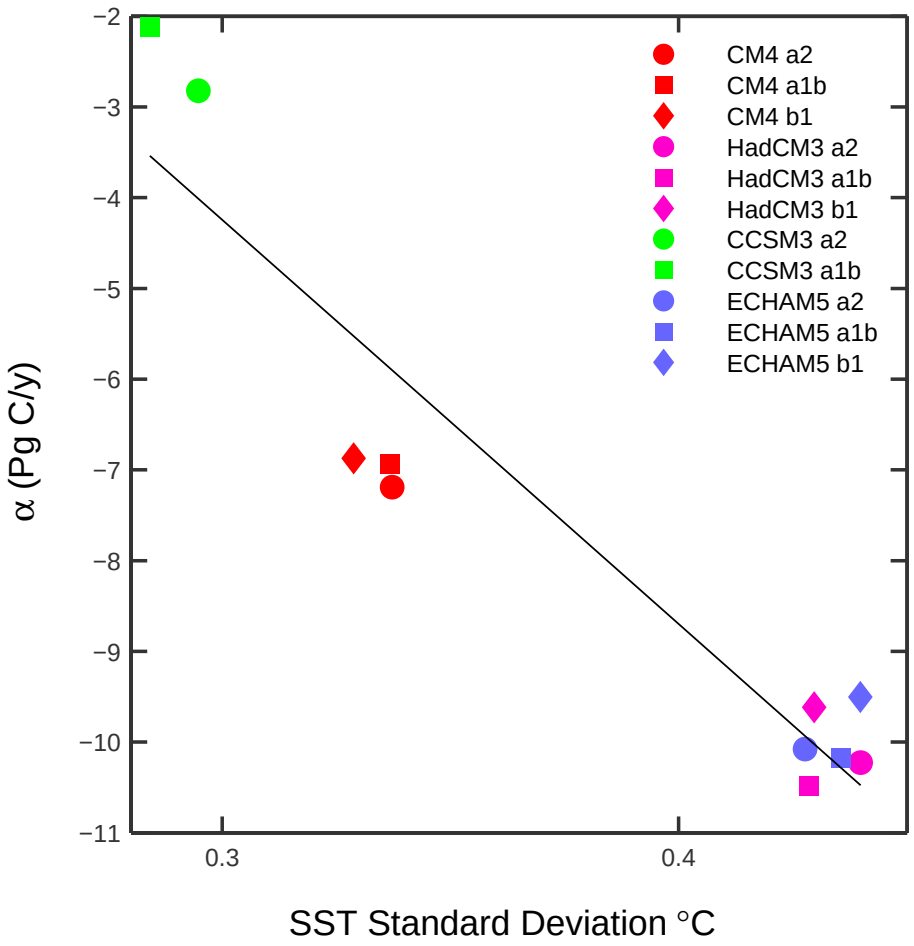

Fig. 4. Relation between the simulation-specific parameter α and global SST variability.

BGD
9, 13685–13712, 2012

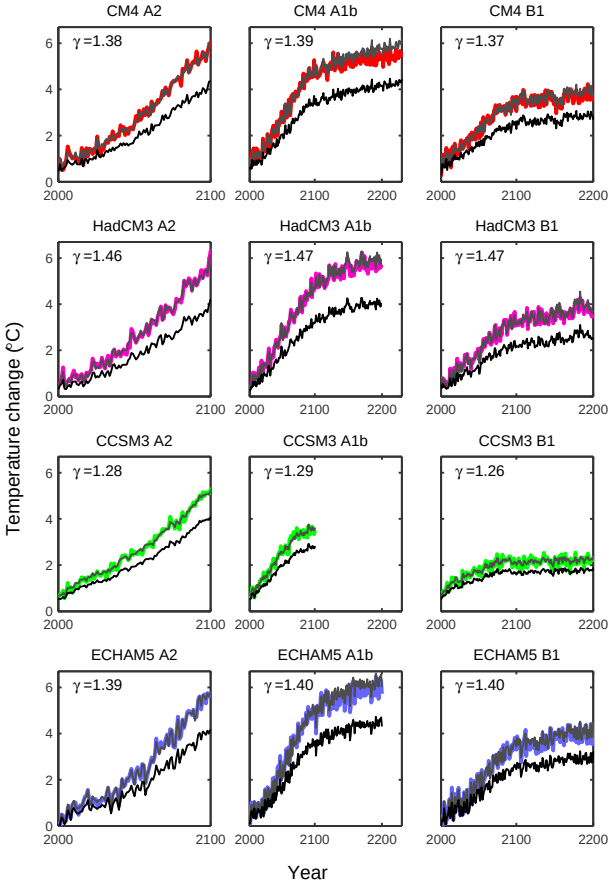

Fig. 5. Average global temperature change, ΔGT (black), average global land temperature change ΔLT (colours) and average global land temperature estimated by $\gamma^{*}\Delta$GT (grey).

BGD
9, 13685–13712, 2012

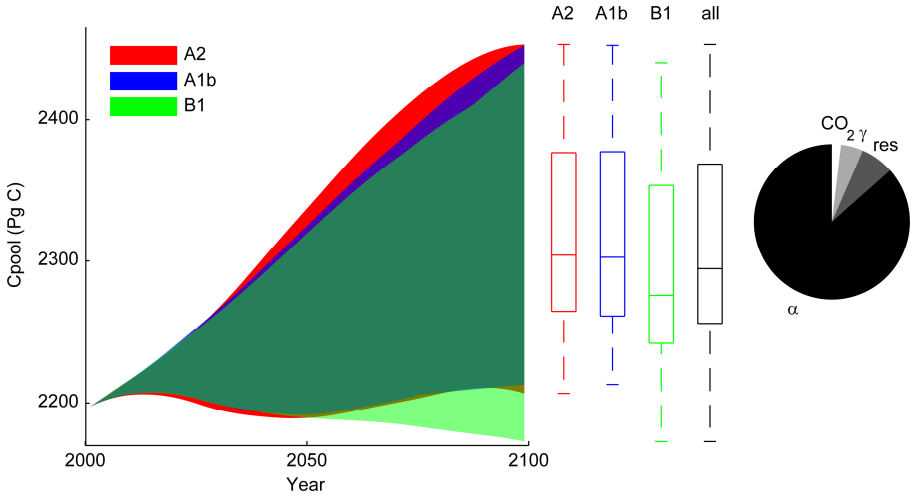

Fig. 6. Results of the 192 replacement model simulations using "artificial GCM" input. The total spread of the A2 scenario simulations in total terrestrial carbon pool (Cpool) is illustrated in red. Blue shows the A1B scenario and green the B1 scenario. The boxplots show the median, 25th and 75th percentile, and maximum and minimum values of the 2099 total terrestrial carbon pool (PgC), for each CO_2 scenario and all simulations. The pie chart shows the proportion of 2099 total carbon pool variability explained by, α, γ, CO_2 scenarios and residual unexplained variation (res).

BGD
9, 13685–13712, 2012